

# Volcanoes and ENSO in millennium simulations: global impacts and regional reconstructions in East Asia

Dan Zhang · Richard Blender · Klaus Fraedrich

Received: 19 December 2011 / Accepted: 2 May 2012 / Published online: 26 May 2012  
© Springer-Verlag 2012

**Abstract** The impacts and cooperative effects of volcanic eruptions and ENSO (El Niño/Southern Oscillation) are analyzed in a millennium simulation for 800–2005 AD using the earth system model (ESM) ECHAM5/MPIOM/JSBACH subject to anthropogenic and natural forcings. The simulation comprises two ensembles, a first with weak (E1, five members) and a second with strong (E2, three members) variability total solar irradiance. In the analysis, the 21 most intense eruptions are selected in each ensemble member. Volcanoes with neutral ENSO states during two preceding winters cause a global cooling in the year after eruptions up to  $-2.5^{\circ}\text{C}$ . The nonsignificant positive values in the tropical Pacific Ocean indicate an El Niño-like warming. In the winter after an eruption, warming is mainly found in the Arctic Ocean and the Bering Sea in E2 warming extends to Siberia and central Asia. The recovery times for the volcano-induced cooling (average for 31 eruptions) vary globally between 1 and 12 years. There is no significant increase of El Niño events after volcanic eruptions in both ensembles. The simulated temperature and the drought indices are compared with corresponding reconstructions in East Asia. Volcanoes cause a dramatic cooling in west

China ( $-2^{\circ}\text{C}$ ) and a drought in East China during the year after the eruption. The reconstructions show similar cooling patterns with smaller magnitudes and confirm the dryness in East China. Without volcanoes, El Niño events reduce summer precipitation in the North, while South China becomes wetter; La Niña events cause opposite effects. El Niño events in the winters after eruptions compensate the cooling caused by volcanoes in most regions of China (consistent with reconstructions), while La Niña events intensify the cooling (up to  $-2.5^{\circ}\text{C}$ ). The simulated and reconstructed drought indices show tripole patterns which are altered by El Niño events. The simulated impact of the Tambora eruption in 1815, which caused the “year without summer” of 1816 in Europe and North America and led to coldness and famines in the Chinese province Yunnan, depends crucially on the ENSO state of the coupled model. A comparison with reconstructed El Niño events shows a moderate cool climate with wet (in the south) and extreme dry anomalies (in the north) persisting for several years.

## 1 Introduction

Volcanic eruptions are major external climate perturbations on the inter-annual time scale with stratospheric dust veils reducing temperature for years and altering summer precipitation patterns globally (Angell and Korshover 1985; Dai et al. 1991; Robock 2000; Santer et al. 2001; Fischer et al. 2007; Robock et al. 2008; D’Arrigo et al. 2009; Timmreck et al. 2009). The most intense eruptions are detectable in the temperature record while impacts on precipitation and pressure are less clear (Mass and Portman 1989; Shindell et al. 2004; Schneider et al. 2009). Winter temperatures after eruptions are above normal in North America and Eurasia whereas North Africa and

---

D. Zhang · R. Blender (✉) · K. Fraedrich  
Meteorological Institute, University of Hamburg,  
KlimaCampus,  
Hamburg, Germany  
e-mail: richard.blender@zmaw.de

D. Zhang  
Institute of Geographic Sciences and Natural Resources Research,  
Chinese Academy of Sciences,  
Beijing, China

D. Zhang  
Graduate School of the Chinese Academy of Sciences,  
Beijing, China

Southeast Asia are cooler (Robock and Mao 1995; Thompson 1995; Robock 2000; Shindell et al. 2003; Schneider et al. 2009). However, while the majority of analyses of the post-volcanic climate pertain to Europe and North America, less is known about China/East Asia although there is a wealth of reconstructions and documentary sources (for a review on volcanic impacts during 1200–1700 AD see Atwell 2001; Yoshimori et al. 2005). In Northeast China, a cooling and drying is found after volcanic eruptions (Mao et al. 2009). In Southeast Asia, there are transitions from wetter towards drier conditions (Anchukaitis et al. 2010) and a drought in East China during the eruption and the subsequent year (Schneider et al. 2009; Peng et al. 2010). The data in this region are useful to validate atmosphere–ocean general circulation model (AOGCM) simulations of volcanic eruptions (see the concerns noted by Anchukaitis et al. 2010).

Large volcanic eruptions inject sulfur gases into the stratosphere, which convert to sulfate aerosols with an e-folding residence time of about 1 year, and the resulting disturbance to the Earth's radiation balance affects surface temperatures as well as the atmospheric circulation (Robock 2000; Robock et al. 2008). Climate recovery time scales after volcanic eruptions are determined by the memory of land surfaces and oceans, and of the carbon cycle, which causes a multi-decadal decrease in atmospheric CO<sub>2</sub> (Froelicher et al. 2011). Robock and Mao (1995) find a time scale of 2 years in 140 year observations. In a model simulation, Robock and Liu (1994) detect a time scale of 4 years for the relaxation of temperature to climatological means and less than 3 years for precipitation. Crowley et al. (2008) assume a 10-year recovery time scale for the ocean mixed layer in an analysis of the cumulative effect of sequences of eruptions during the nineteenth century. During the Dalton minimum (1790–1830) at the end of the Little Ice Age, a series of volcanic eruptions occurred which lowered temperature persistently since the oceanic mixed layer could not recover from the previous eruption (Crowley et al. 2008; Cole-Dai et al. 2009). After the most intense volcanic eruptions of the last millennium in 1258 (unknown) and in 1815 (Tambora), the cold temperature anomalies recovered on decadal time scales, which is attributed to the ocean heat uptake in a coupled ensemble experiment (Stenchikov et al. 2009) and the carbon cycle feedback in the present model configuration (Brovkin et al. 2010; Froelicher et al. 2011).

Volcanic eruptions and El Niño/Southern Oscillation (ENSO) events can influence the climate on similar time scales and with comparable magnitudes. The combined signal can be greater in magnitude with different geographical patterns than suggested from a simple linear combination (Kirchner and Graf 1995). Furthermore, an increase of the probability of El Niño events after volcanic eruptions is detected in reconstructions (Adams et al. 2003; McGregor et al. 2010), although an association between low-latitude

volcanic events and lower sea surface temperature (SST) in the tropical oceans is also found (D'Arrigo et al. 2009). Enhanced probability of occurrences for El Niños after eruptions is supported by simulations with the Zebiak–Cane model (Mann et al. 2005; Emile-Geay et al. 2008); however, uncertainties remain, which are associated with the minimum intensity of eruptions and the enhancement of their likelihood (Emile-Geay et al. 2008). This impact is highly relevant for Southeast Asia since ENSO is related to drought during El Niño and wetness during La Niña phases; thus, both phenomena can lead to either a partial cancellation or to an enhancement with even more disastrous consequences. Since reliable reconstructions of past El Niño events are restricted to the last three centuries (Quinn 1993), AOGCM simulations are necessary to retrieve correlations and possible causal relationships.

The eruption of the Tambora in 1815 was the most intense in historic times (Rampino and Self 1982; Stothers 1984) and caused the “year without summer” in North America and Europe with dramatic consequences for food supply and health (Oppenheimer 2003; Soon and Yaskell 2003). As a major eruption located in the tropics (D'Arrigo et al. 2009), the Tambora impact was global (Robock 2000). Chinese documentary sources describe disasters in various regions after 1815 (Yang et al. 2005): in the province of Yunnan (in the South), there was a 3-year famine (1815–1817) due to a poor harvest of rice and maize caused by low summer and autumn temperatures (anomalies range  $-2$  to  $-3^{\circ}\text{C}$ ). In the eastern parts of China including the Yangtze River catchment, cold anomalies have also been found, but famines are not documented in these regions. After 1815, frequent and strong fluctuations of wet and arid conditions occurred in China, and increased numbers of floods and droughts are reported in the Yangtze delta (Jiang et al. 2005). Since famines and social disasters might have different causes (warm or cold, wet or dry), an analysis of past temperature and precipitation anomalies on a regional scale yields useful hints to understand the evolution of historical events and to adapt to future natural catastrophes.

Our aims were to assess cooperative effects and impacts of volcanic eruptions and ENSO events in ensemble climate simulations for the last 1,200 years with a complex atmosphere–ocean–land model and to compare it with reconstructions in East Asia (see also Zhang et al. 2011). Section 2 describes the earth system model, the volcanic forcing, the methods, and the reconstructed data. Section 3 presents global patterns of the temperature and precipitation responses to volcanic eruptions without ENSO events. The relaxation time scales of the temperature decay are determined globally by exponential fits. Section 4 focuses on the comparison between simulated and reconstructed temperature and drought indices in East Asia for: (1) volcanic impacts without ENSO events, (2) ENSO impacts without

preceding eruptions, and (3) concurrent eruptions and ENSO events. A focus lies on an analysis of the climate after the Tambora eruption (1815) to detect causes for famines reported in China/Southeast Asia (Section 5). As the eruptions in the ensemble simulations concur with different simulated ENSO states, a selection of an optimal combination is possible by comparing the model's results with documented El Niño events (the selection of optimal ensemble members has been suggested by Goosse et al. 2006). The results are summarized and discussed in Section 6.

## 2 Data and methods

### 2.1 Model, ensemble simulations and data analysis

The millennium simulations are carried out using the COSMOS–Atmosphere–Land–Ocean Biogeochemistry earth system model (ESM, “millennium run”, Jungclaus et al. 2010). The model includes the atmospheric model ECHAM5 (Roeckner et al. 2003), the ocean model MPIOM (Marsland et al. 2003), and modules for land vegetation JSBACH (Raddatz et al. 2007) and ocean biogeochemistry HAMOCC (Wetzel et al. 2006), which are coupled via the OASIS3 coupler. Anthropogenic land use is prescribed (Foley et al. 2003, Pongratz et al. 2008). ECHAM5 is run at T31 resolution ( $\approx 3.75^\circ \times 3.75^\circ$ ) with 19 vertical levels up to 10 hPa. The ocean model MPIOM has a horizontal grid spacing of about  $3^\circ$  with 40 unevenly spaced vertical levels and applies a conformal mapping grid with a horizontal resolution ranging from 22 to 350 km. This grid setup is a low resolution version of the model used for the scenario simulations for the Intergovernmental Panel of Climate Change (IPCC) and the Coupled Carbon Cycle Climate Model Intercomparison Project (Friedlingstein et al. 2006, Jungclaus et al. 2010).

**Ensembles** Two reconstructed total solar irradiance (TSI) forcings for the last 1,200 years are used to produce two ensembles: ensemble E1 (five members) is simulated with the solar irradiance forcing reconstructed by Krivova et al. (2007) with a weak (0.1 %) variation of the standard TSI value of  $1,367 \text{ W/m}^2$  (given by the difference between present day and Maunder Minimum, see Fig. 1a) and a second ensemble E2 (three members) with a more intense variation (0.25 %), comparable to previous reconstructions (for example Bard et al. 2000). Sensitivity experiments in a control run forced with varying solar irradiance only yield a sensitivity of 0.15 K global temperature change per watts per square meter as response to the 11-year cycle (Jungclaus et al. 2010). Recent assessments over the last century arrive at sensitivities between 0.1 and  $0.2 \text{ K/(Wm}^{-2}\text{)}$  (Camp and

Tung 2007; Lean and Rind 2008), and over the last 60 years between 0.12 and  $0.17 \text{ K/(Wm}^{-2}\text{)}$  (Tung et al. 2008). Thus, the model's sensitivity is well in the range of observational estimates. Zhang et al. (2010) compared both ensembles with climate reconstructions in China and concluded that ensemble E1 reproduces the reconstructed climate variability; therefore, the present analysis is restricted to this five-member ensemble E1 unless indicated otherwise.

**Volcanic forcing** Volcanic forcing is represented in terms of the aerosol optical depth at  $0.55 \mu\text{m}$  and of the effective radius distribution (Crowley et al. 2008). In the simulation (Jungclaus et al. 2010), this forcing is resolved in four latitude bands ( $30^\circ\text{--}90^\circ \text{ N}$ ,  $0^\circ\text{--}30^\circ \text{ N}$ ,  $0^\circ\text{--}30^\circ \text{ S}$ , and  $30^\circ\text{--}90^\circ \text{ S}$ ) with a temporal resolution of 10 days (Fig. 1b, c). The volcanic eruptions start in January if the exact date is unknown. In the annual forcing series, 21 large volcanic eruptions are defined for each member in ensembles E1 and E2 (see Table 1, 105 eruptions in total in E1 and 63 in E2) based on the strongest reduction in net top solar radiation (for a detailed review on past eruptions, see Newhall and Self 1982; Peng et al. 2010; Global Volcanism Program, Smithsonian National Museum of Natural History/Washington 2011). The lowest reduction in this set is  $-2.0 \text{ W/m}^2$  caused by Santa Maria in Guatemala in 1903 (average of all eight members), which is slightly larger than the observed reduction of  $-1.7 \text{ W/m}^2$ . The highest reduction with values between  $-16.4$  and  $-16.9 \text{ W/m}^2$  in all eight members is caused by the volcanic eruption in 1258 (unknown volcano). Brovkin et al. (2010) found a global temperature drop of 1 K for this eruption and a relaxation time of 10 years within the present model setup. As in Peng et al. (2010), the year with the largest reduction in irradiance is defined as the volcanic eruption year. This definition can lead to a discrepancy between the historic and simulated eruption years in the present analysis, since the aerosol layer accumulates leading to a delayed response. A particular scheme for the removal of clustered eruptions is not implemented since there are only two pairs of eruptions within the recovery time scale which is below 3 years in China except for the northeast (eruptions pairs in 1809–1816 and 1832–1835, see Table 1 and recovery time scales in Fig. 5b). Intensities and latitudes of the volcanoes are not considered.

**ENSO** The ENSO index is defined by the principal component time series (PC1) of the first EOF of the tropical Pacific SST variability in winter (DJF) and denoted as PC1-SST (see Hoerling et al. 2001). El Niño events are given for  $\text{PC1-SST} > 1$ , La Niña events for  $\text{PC1-SST} < -1$ , and a neutral state for  $|\text{PC1-SST}| < 1$ . The problem of removing ENSO-related variations from climate records has been addressed in previous studies

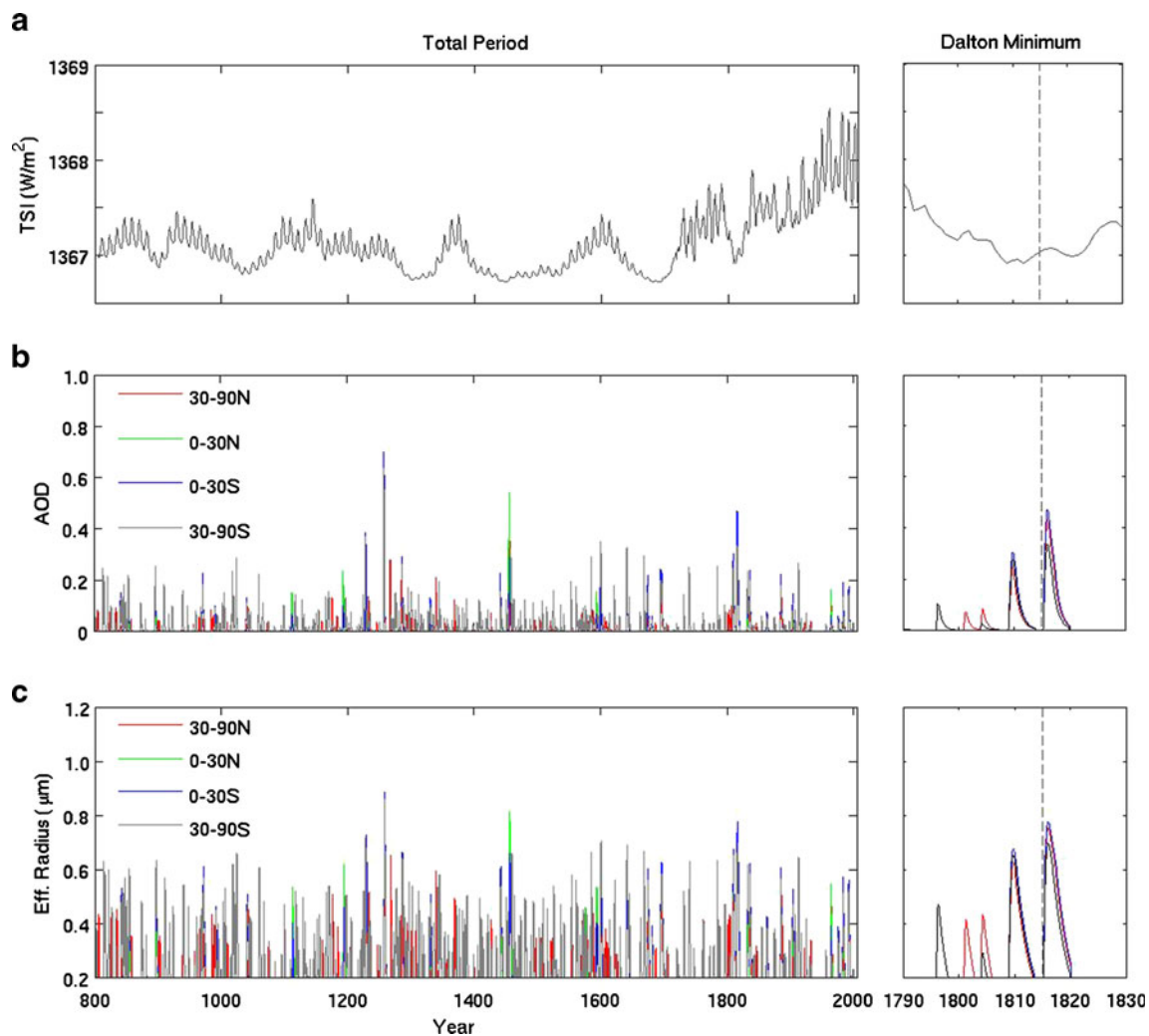


**Fig. 1** a Annual mean total solar irradiation in ensemble E1 for the whole simulation period (*left panel*) and the Dalton Minimum (1790–1830, *right panel*) based on the reconstruction by Krivova et al. (2007);

**b** aerosol optical depth (dimensionless fraction); and **c** effective radius [in micrometers]; in **b** and **c**, latitude belts are separated. The Dalton Minimum includes the Tambora eruption in 1815

using a variety of methods (see for example Penland and Matrosova 2006; Compo and Sardeshmukh 2010). Here the two ensemble simulations with eight members allow the identification of a sufficient number of intense eruptions with different ENSO responses. A simple and straightforward method is used to avoid years with overlaps: First the response of climate during the year after an eruption for neutral ENSO states ( $|\text{PC1-SST}| < 1$ ) in two preceding winters is considered. Secondly, the ENSO impact is determined during years without preceding eruptions. The final analysis considers years with concurrent eruptions and ENSO events. To determine the cooperative effects of volcanic eruptions and ENSO anomalies, a composite analysis of surface temperature and precipitation are performed in the year after the eruption (if not indicated otherwise).

**Standardized Precipitation Index** In the present publication, simulated precipitation anomalies are analyzed in terms of the Standardized Precipitation Index (SPI, McKee et al. 1993). To obtain this index, the monthly precipitation is transformed to a standard normal distribution to yield monthly SPI values by preserving probabilities, which ensures that the SPI gives a uniform measure for dryness and wetness in different climate regimes. In the analysis, we use the monthly time scale characterizing the meteorologically relevant period; the summer SPI is the average of the monthly SPI in June, July, and August (JJA) (see Bordi et al. 2004, Sienz et al. 2007 and Zhu et al. 2010, for a detailed method description and classification). Sims et al. (2002) suggest that the SPI is a better indicator for short-term precipitation anomalies and soil wetness than the Palmer Drought Severity Index (PDSI), while Zhai et al. (2010) suggest

**Table 1** List of the 21 selected volcanic eruptions in 800–2005 in the model simulations (the eruption year is defined by a decrease in net top solar irradiation of at least  $-2.0 \text{ W/m}^2$ )

No.	Year	Name	VEI
1	842	Unknown	
2	854	Unknown	
3	897	Unknown	
4	971	Unknown	
5	1193	Unknown	
6	1228	Unknown	
7	1258	Unknown	
8	1286	Unknown	
9	1442	Unknown	
10	1456	Pinatubo?	6
11	1600	Huaynaputina	6
12	1641	Parker	6
13	1673	Gamkonora	
14	1694	Serua?/Hekla?	
15	1809	St. Helen?	
16	1815	Tambora	7
17	1832	Babuyan Claro	4?
18	1835	Cosiguina	
19	1884	Krakatau	6
20	1903	Santa Maria/2 others	4
21	1992	Pinatubo	6

The Volcanic Explosivity Index (VEI) is included and question marks indicate uncertainty (Newhall and Self 1982; Peng et al. 2010; Global Volcanism Program, Smithsonian National Museum of Natural History/Washington 2011). The method used to separate volcanic eruptions with and without ENSO events see Section 2 for a detailed description

that PDSI and SPI can be used to describe dryness and wetness. Surface temperature and SPI anomalies are computed with respect to the time means which are determined individually for each ensemble member in the whole period 800–2005.

## 2.2 Reconstructions

The reconstructed temperature used in the present analysis is from Mann et al. (2009) in 800–2005 (the complete period is 500–2006). The reconstructed drought index during summer (JJA, from 1300–2005) is defined by the PDSI based on tree rings in the forested areas of the Asian Monsoon area (Cook et al. 2010). All anomalies are taken with respect to the time means in the corresponding data set during the whole period.

The volcanic eruptions are selected based on Ammann et al. (2007), Ammann and Naveau (2003), and Fischer et al. (2007); the event years with reconstructed El Niño are based on Gergis and Fowler (2006, see Table 2). The lists are denoted using the initial of the first author plus the number of event years, e.g., the first list is denoted “A15” according

to Ammann et al. (2007) with 15 eruption years. The anomalies refer to the whole time period.

The reconstructed temperature time series used in Section 5 are from Wang et al. (2007), Ge et al. (2003), and Yang et al. (2002). Data from Wang et al. (2007) are reconstructed for 1000–2005 AD with 10-year resolution, data from Ge et al. (2003) are in 800–1999 AD with 30-year resolution (10-year resolution in 960–1100, the complete reconstructed period is 15–1999 AD), and data from Yang et al. (2002) are for 800–1999 AD with 10-year resolution (the complete reconstructed period is 0–1999 AD).

The reconstructed drought index time series used in Section 5 are from the Central Meteorological Bureau (1981, hereafter CMB), Zheng et al. (2006), and Cook et al. (2010). The annual drought index by CMB is reconstructed for 1470–1979 (May–September) compiling reports about the weather found in local gazettes in 120 districts in China. The annual drought index by Zheng et al. (2006) is reconstructed for 501–2000 in eastern parts of China based on Chinese historical documents and instrument measurements. The summer PDSI (JJA) by Cook et al. (2010) for 1300–2005 is reconstructed based on tree rings in the forested areas of the Asian monsoon area (see Cook et al. 2010 for details).

## 3 Global impacts of volcanoes

The global climate response during the year after a volcanic eruption is considered without ENSO events (neutral PC1-SST) in the two preceding winters, which leads to 31 eruption years in total in ensemble E1 (22 in E2).

### 3.1 Temperature and SPI

Volcanoes cool the northern hemisphere in North America and Eurasia during the year following the eruption years (Fig. 2). Areas with weak positive amplitudes are found in the tropical Pacific, the Bering Sea, and in parts of the Antarctic Ocean. Here, the nonsignificant positive values in the tropical Pacific Ocean indicate an El Niño-like warming, which is consistent with Adams et al. (2003). Significant areas marked by “X” are based on the Mann–Whitney test at the 95 % level.

The response pattern of the SPI is more complex than temperature. Drier conditions are found in central Asia, East China, Australia, and North Africa. Drier ocean basins are in the east and the northwest Pacific, the central Atlantic, and the Antarctic Ocean. In the central Pacific, both drier and wetter conditions occur.

Stenchikov et al. (2006) observe warming in Eurasia for two winters following the eruption which appears to be weaker in the nine models used in the IPCC Fourth

**Table 2** List of volcanic eruptions with and without El Niño events used for the reconstructed temperature anomalies and the Palmer Drought Severity Index (PDSI) in summer (JJA)

Type	Volcanoes			Volcanoes with El Niño <sup>a</sup>			
	A15 <sup>b</sup> /A10 <sup>c</sup>		AN46 <sup>d</sup>	F12 <sup>e</sup>	A1 <sup>b</sup>	AN7 <sup>d</sup>	F2 <sup>e</sup>
Name	A15 <sup>b</sup> /A10 <sup>c</sup>		AN46 <sup>d</sup>	F12 <sup>e</sup>	A1 <sup>b</sup>	AN7 <sup>d</sup>	F2 <sup>e</sup>
No.	15/10	46		12	1	7	2
Years	<i>1258</i>	1443 1665 1815	1596	1903	1586	1586	
	<i>1259</i>	1452 1674 1823	1600		1619	1903	
	<i>1269</i>	1459 1680 1831	1641		1660		
	<i>1278</i>	1463 1693 1835	1673		1737		
	<i>1279</i>	1490 1712 1861	1809		1890		
	1452	1504 1721 1880	1815		1902		
	1453	1512 1728 1883	1823		1903		
	1600	1522 1744 1911	1831				
	1601	1554 1749 1928	1835				
	1641	1568 1752 1953	1883				
	1809	1571 1760 1963	1963				
	1810	1595 1774 1968	1982				
	1815	1600 1789 1974					
	1816	1605 1794 1982					
	1884	1622 1808					
		1641 1813					

The sources for volcanic eruptions are

<sup>a</sup> The event years with reconstructed El Niño are according to Gergis and Fowler (2006)

<sup>b</sup> Ammann et al. (2007)

<sup>c</sup> While the data are available after 1250, the reconstructed PDSI starts from 1300 (missing years in italics)

<sup>d</sup> Ammann and Naveau (2003)

<sup>e</sup> Fischer et al. (2007)

Assessment Report. In our simulation, warming in the following winter is found in both ensembles in the Arctic Ocean, the Bering Sea, the tropical Pacific, and the Southern Pacific Ocean between 180° and 120° W

(Fig. 3a, b). The warming in Eurasia, which is evident in observations (Stenchikov et al. 2006) and reconstructions (Fischer et al. 2007), is only partly simulated. In the east of the continent, both ensembles show a weak warming. However, the expected warming over Europe is not simulated, which is a hint that the model is not able to simulate the dynamical response of the North Atlantic Oscillation (NAO) in a correct way (positive phase of the NAO after an eruption, see e.g., Stenchikov et al. 2006). The simulated warming (nonsignificant) in the tropical Pacific Ocean is similar to the observed data (Stenchikov et al. 2006), which is attributed to a net sampling of positive ENSO phases in the composite. Notice that our list of volcanic eruptions excludes the eruptions with concurrent ENSO events. In the second winter, the warming areas shrink in ensemble E1 but remain in E2 (in the Arctic Ocean). Note that the individual ensemble members show different amplitudes of warming.

### 3.2 Recovery time scales

In the present analysis, the recovery of the local temperature drop after an eruption is described in terms of an exponential decay,  $\Delta T(t) = \Delta T_0 \exp(-t/\tau)$ , beginning with the first year after the eruption  $t=0$  (see Fig. 4 for two examples of fitted temperature episodes). At every grid box, the amplitude  $\Delta T_0$  and the time scale  $\tau$  are fit parameters for the averages of the temperature relaxation anomalies following 31 eruptions.

The fitted decay amplitudes  $\Delta T_0$  and the relaxation timescales  $\tau$  are shown in Fig. 5a, b at grid points where fits can be achieved (fits require a negative amplitude and a sufficient decay of the anomalies). Areas marked by X have an *R*-square value above 0.4 (goodness-of-fit statistics at the 95 % level). Large amplitudes  $\Delta T_0$  reaching  $-2^\circ\text{C}$  are found in North America, the Himalaya, and the Barents Sea, and in the southern Pacific Ocean between 160° and 60° W. Land and ocean reveal similar amplitudes. Areas with negligible amplitudes inhibit fits (void in Fig. 5a, b); furthermore, areas with weak positive

**Fig. 2** **a** Annual mean temperature anomalies (in degree Celsius) and **b** summer SPI (JJA) in the ensemble E1 in the year after volcanic eruptions without ENSO events (neutral,  $|\text{PC1-SST}| < 1$ ). Significant areas are marked (95 % level)

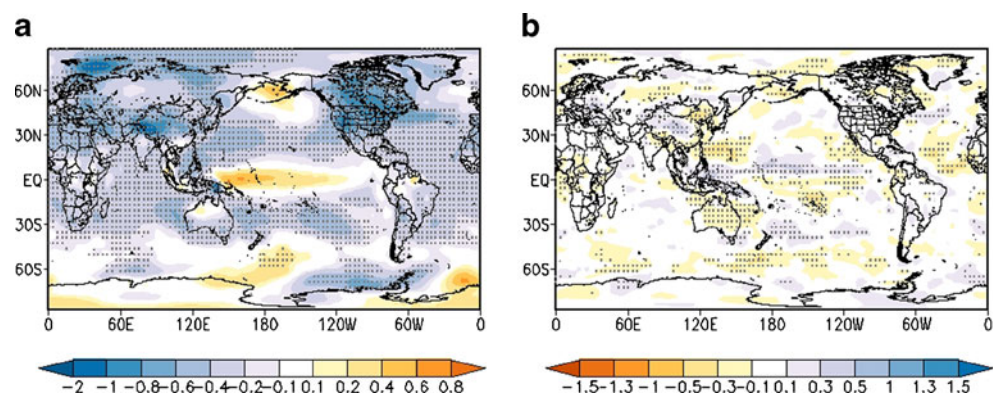
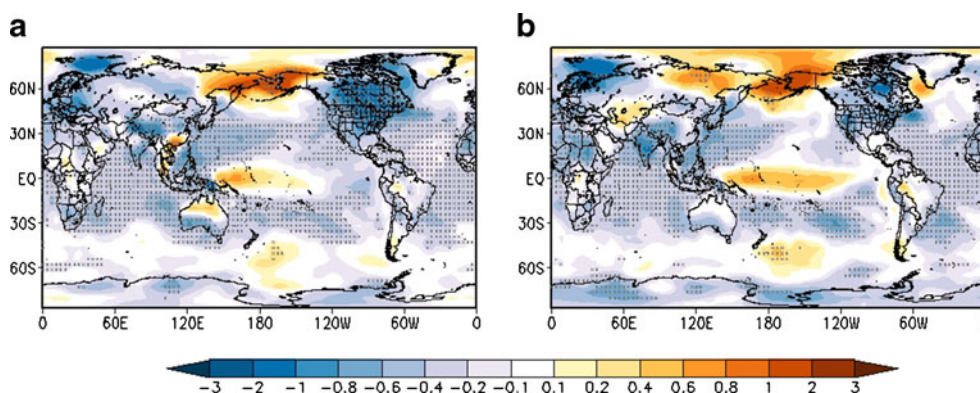


**Fig. 3** Winter temperature anomalies (in degree Celsius) after volcanic eruptions without ENSO events (neutral,  $|PC1-SST| < 1$ ) in ensembles **a** E1 and **b** E2. Significant areas are marked (95 % level)



amplitudes (mostly in the tropical Pacific, the Bering Sea, and in parts of the southern Pacific, as in Fig. 2a) are excluded. Ensemble E2 reveals similar results (not shown). Note that this amplitude is the result of a fit and not identical to the anomaly during the year after the eruption (Fig. 2a).

Long-lasting influence with recovery time scales  $\tau$  up to a decade is found in southern Europe, Northeast China, and in the Arctic Ocean (Fig. 5b). In China, the time scales are mostly within 1–4 years and reach 10 years in the northeast. A remarkable coincidence of high amplitudes

and large time scales appears in the southern Pacific Ocean.

One of the possible mechanisms for the small amplitudes in the ocean basins is rapid mixing in the surface layer (for example in the North Atlantic where small amplitudes inhibit fits at some grid points). In regions with small amplitudes, intense long-term memory has been identified in preceding analyses of the global sea surface temperature (Fraedrich and Blender 2003; Fraedrich et al. 2009). On the continents, the snow albedo feedback is a possible cause for long relaxation times; furthermore, soil wetness and permafrost may induce long memory. Since the snow cover on the Himalaya reveals short time scales (see Fig. 5a, b), the interpretation of long relaxation time scale as a snow albedo feedback is unclear.

#### 4 East Asia: volcanic and ENSO impacts

After the analysis of volcanic impacts on a global scale (Section 3), this section presents an analysis of the impacts and the cooperative effects of volcanic eruptions and ENSO events in simulations and reconstructions in East Asia.

##### 4.1 Volcanic impacts without ENSO events

Volcanoes cool East Asia, especially the high altitude Himalayan region in west China with anomalies as low as  $-2^{\circ}\text{C}$  during the year after eruptions (Fig. 6a, b). Significant changes marked X are based on the Mann–Whitney test (95 %). The mean over China is  $-0.54^{\circ}\text{C}$  ( $-0.53^{\circ}\text{C}$  in ensemble E2). These anomalies are larger than twice the standard deviation.

Although the simulated cooling pattern is in agreement with the reconstructions (Mann et al. 2009), the simulated amplitudes are larger (Fig. 6c–e). This can partly be explained by the low threshold for the intensity of volcanic eruptions used for reconstructions compared with simulations (compare Tables 1 and 2). Sporadic weak warming is found in Northwest China and central Asia for the volcanic eruption

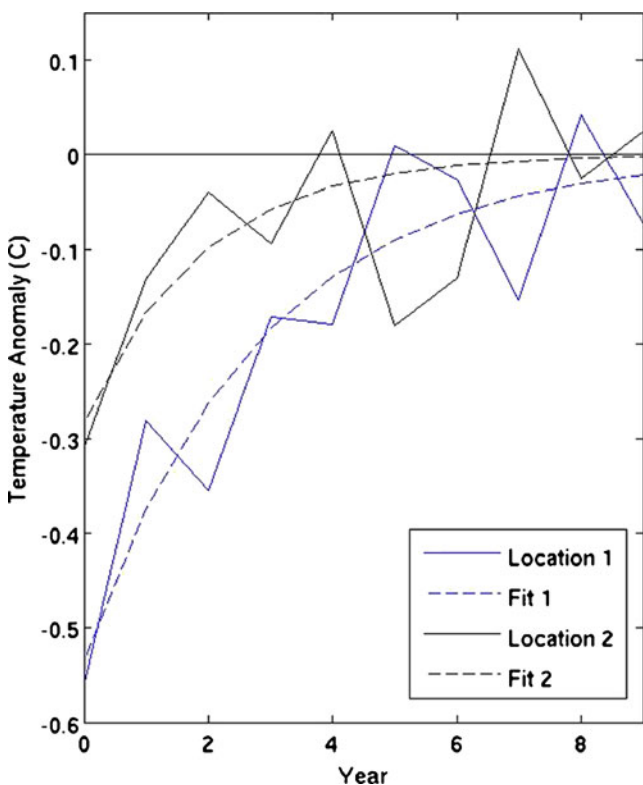
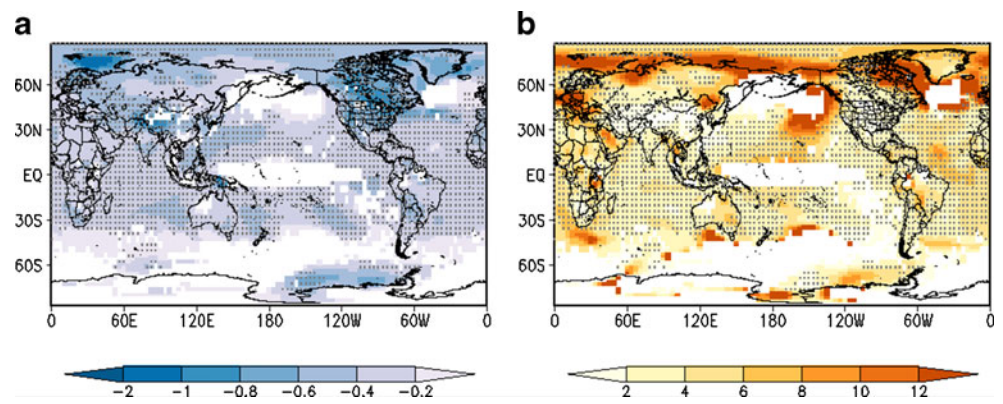


**Fig. 4** Examples of exponential fits to the averaged temperature decay. Location 1,  $102^{\circ}\text{E}/22^{\circ}\text{N}$  (Northeast China, recovery time scale  $\tau \approx 3$  years,  $\Delta T_0 \approx -0.5^{\circ}\text{C}$ ); location 2,  $116^{\circ}\text{E}/43^{\circ}\text{N}$  (Southwest China,  $\tau \approx 2$  years,  $\Delta T_0 \approx -0.3^{\circ}\text{C}$ )

**Fig. 5** **a** Temperature amplitude  $\Delta T_0$  (in degree Celsius) and **b** relaxation time scale  $\tau$  (in years) of the temperature decay averaged after 31 volcanic eruptions in ensemble E1 without ENSO events (neutral,  $|\text{PC1-SST}| < 1$ ) during the preceding two winters. In the void areas, fits cannot be achieved since a negative amplitude and a sufficient decay of the anomaly are required (see text for details). Significant areas are marked by “X” (95 % level)



lists A15 and AN46 (Fig. 6c, d) and a significant warming for F12 (Fig. 7e), which is missing in the simulations (Fig. 6a, b).

Central China experiences anomalous wet summer (JJA) conditions while a weak dryness prevails in the south and the northeast of China (Fig. 7a, b). The average summer rainfall anomaly in China during the year after the eruption is  $-56$  mm/month in E1 ( $-43$  mm/month in E2). Mao et al.

(2009) reported cool and dry periods after 11 volcanic eruptions. The rainfall deficit after the eruption year is 85 % significant in our analysis (a rainfall anomaly is also found by Anchukaitis et al. (2010) and Peng et al. (2010)).

The reconstructed drought index (Cook et al. 2010) shows drier conditions in most parts of China (significant in west China for list A10, in the North China Plain for

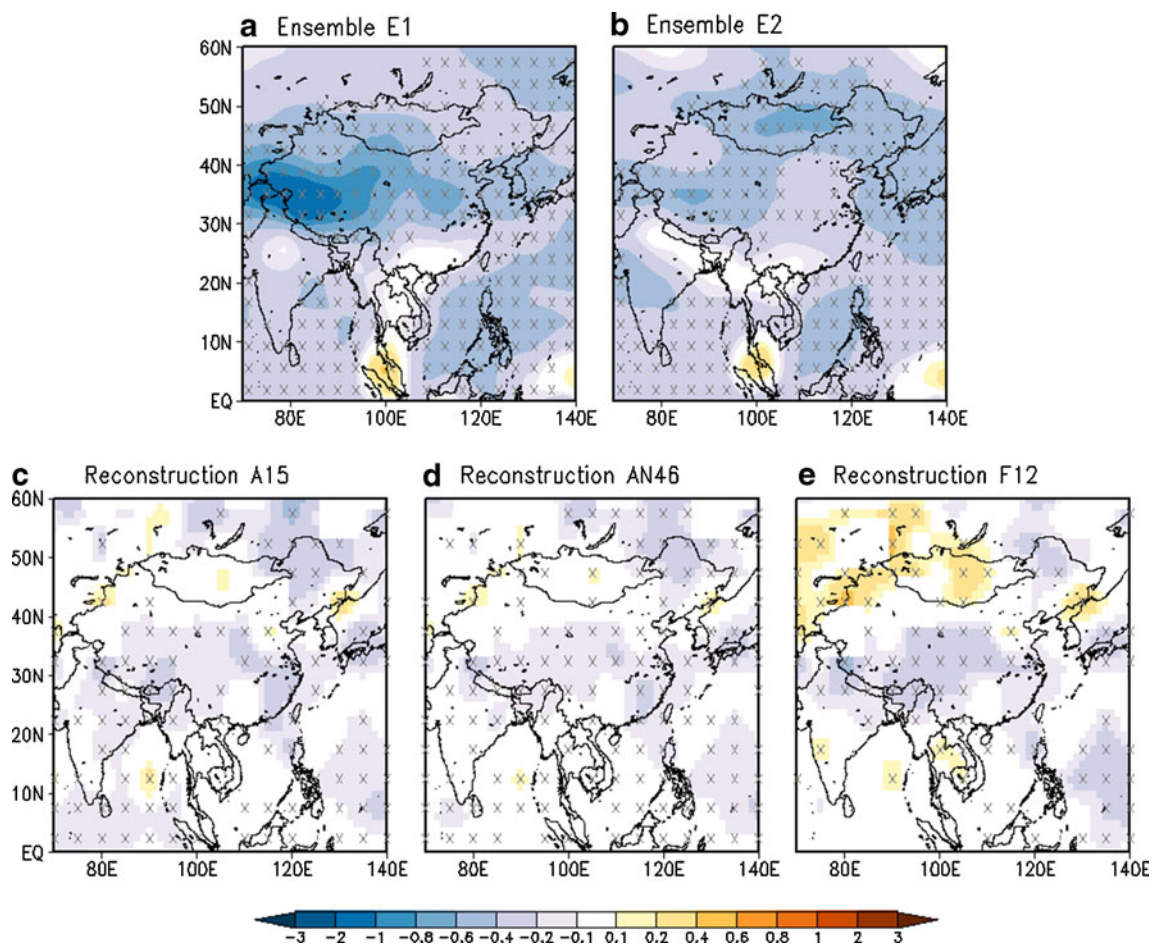


**Fig. 6** Annual mean temperature anomalies (in degree Celsius) in simulations **a** ensemble E1 and **b** ensemble E2 after volcanic eruptions without ENSO events in two preceding winters (neutral,  $|\text{PC1-SST}| < 1$ ); and in reconstructions according to the list **c** A15

(Ammann et al. 2007); **d** AN46 (Ammann and Naveau 2003); and **e** F12 (Fischer et al. 2007, see Table 2) in the year after volcanic eruptions without El Niño events in the preceding winter. Significant areas are marked (95 % level)

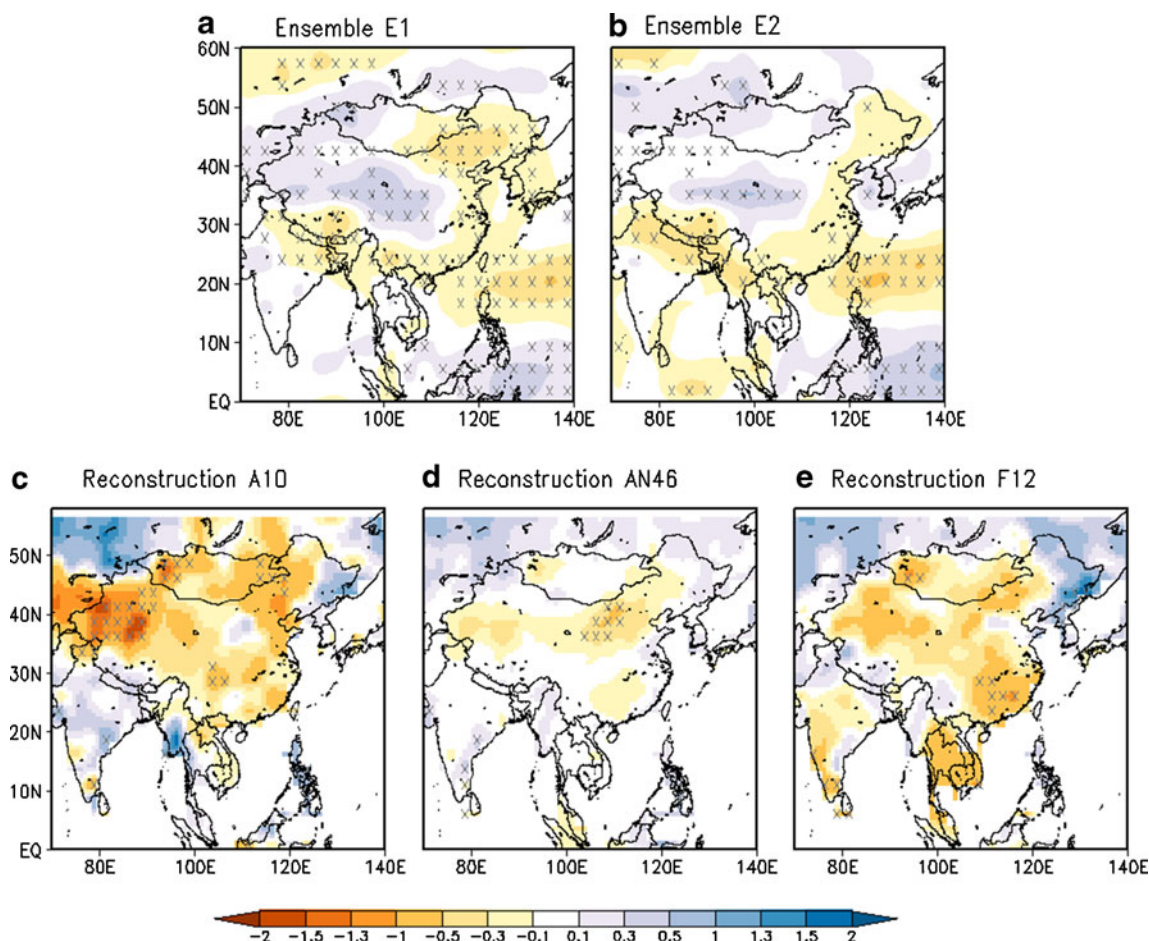


**Fig. 7** Same as Fig. 6 for (a, b) the simulated summer (JJA) mean of the monthly Standardized Precipitation Index (SPI), and c–e the reconstructed summer (JJA) mean of the Palmer Drought Severity

Index (PDSI) according to the list: c A10 (Ammann et al. 2007); d AN46 (Ammann and Naveau 2003); and e F12 (Fischer et al. 2007, see Table 2)

AN46 and in Northeast China for F12, Fig. 7c–e). In India, there is nonsignificant wetness except for list F12. Discrepancies occur in west China and central Asia with significant wetter conditions in simulations (compare Fig. 7a, b). While the wetness in India is also found in simulations, the dryness in parts of Southeast Asia cannot be confirmed by reconstructions according to the three lists. Possible causes for the discrepancies are (1) that the direct influence of the reduction in shortwave radiation due to aerosol forcing on monsoon circulation (precipitation) is offset or overwhelmed by indirect or dynamical influences in reconstructions (suggested by Anchukaitis et al. 2010) or (2) the uncertainty of the parameterization of aerosol microphysics identified by Timmreck et al. (2010).

#### 4.2 ENSO impacts without preceding eruptions

In the analysis of the ENSO impact, we exclude the years with a preceding volcanic eruption. The impacts of winter El Niño and La Niña events on temperature and precipitation anomalies in the subsequent year are almost anti-symmetric

(determined in ensemble E1, Fig. 8a–e). This anti-symmetric image is consistent with Hagemann et al. (2006), supporting the view that inter-annual variations of precipitation at lower latitudes are largely driven by SST anomalies in the equatorial Pacific. El Niño warms the largest part of East Asia except for the northeast, for example in India and Southeast Asia temperature anomalies up to +1°C are simulated (opposite for La Niña, Fig. 8a, b). The summer mean SPI for El Niño events shows a tripole pattern oriented from southwest to the northeast (Fig. 8d, e), whereas Southeast Asia experiences moderate summer wetness, India and Northeast China are drier (the La Niña impact is almost opposite). Clearly, the dominant impact is in the western tropical Pacific.

#### 4.3 Volcanic impacts with ENSO events

To assess whether volcanic eruptions are linked to an increase of El Niño events, the numbers of concurrent events are analyzed: among the 105 volcanic eruptions in ensemble E1 (63 in E2), 23 (E2: 12) are accompanied by El

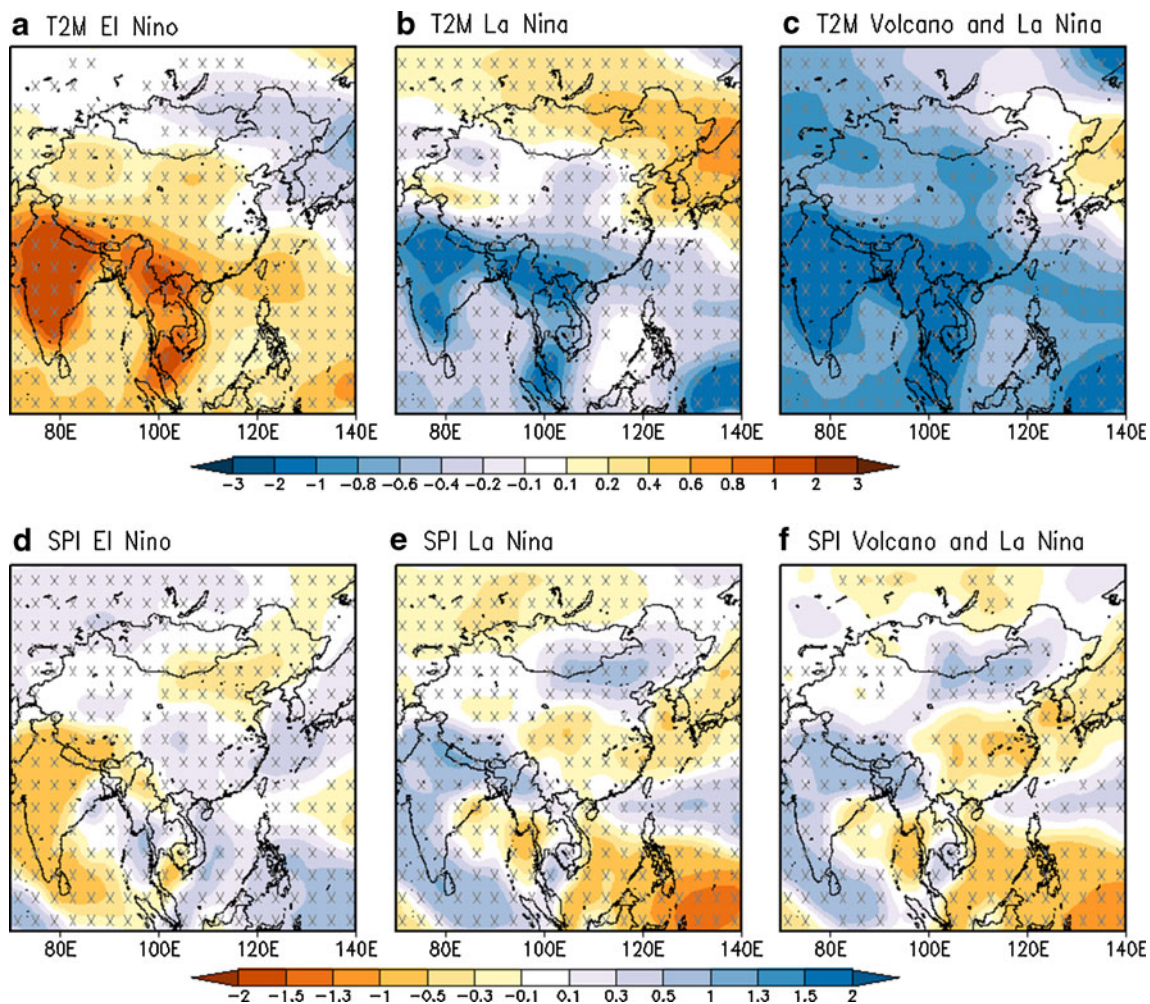


**Fig. 8** Simulated annual mean temperature anomalies (in degree Celsius) in ensemble E1 in the year after **a** El Niño and **b** La Niña events without preceding volcanic eruptions; and **c** volcanic eruptions with La

Niña events; **d–f** summer (JJA) mean of the monthly Standardized Precipitation Index (SPI). Significant areas are marked (95 % level)

Niño events in the following winter (with identical numbers of La Niña events). The sum of El Niño events amounts to 1,249 (733) and La Niña events to 1,164 (704). Since the  $p$  values are 0.81 for El Niños in E1 (E2, 0.84) and 0.59 for La Niñas in E1 (E2, 0.94), we conclude that there is no significant increase of El Niño events after volcanic eruptions in both ensembles.

The simulated temperature and SPI responses during the year after volcanic eruptions with a winter El Niño or La Niña event may reveal dramatic impacts. In China, the cooling effect caused by volcanic eruptions (Fig. 6a, b) is almost compensated by the warming induced by El Niño events (Fig. 9a, b). The superposition of the La Niña and the volcano impact (Fig. 8c) yields enhanced cooling by the same order of magnitude. In the northern Pacific, the La Niña-induced warming dominates. After an eruption with an accompanying El Niño event, the temperature anomaly in ensemble E1 is  $-0.12^{\circ}\text{C}$  (E2,  $-0.31^{\circ}\text{C}$ ) and for a La Niña event  $-0.73^{\circ}\text{C}$  in E1 (E2,  $-0.68^{\circ}\text{C}$ ).

The compensation of the volcanic impacts by El Niño events is also found in reconstructions (Fig. 9c–e), resulting in rather weak anomalies in Northwest China. The Tibetan Plateau and the eastern parts of China remain cold. However, the simulated warming in South Asia (Fig. 9a, b) is missing in all lists: A1, AN7, and F2.

In the present simulations, the cooperative precipitation response of volcanoes and El Niños (Fig. 10a, b) reveals a quasi-linear superposition with a dominance of the El Niño pattern shaped as a tripole (Fig. 8d). In west and central China, wetness caused by volcanic eruptions is unaltered by El Niños; in the north drought is even stronger in the combined case (Fig. 10) than in the pure volcano or El Niño response. A similar superposition pertains to La Niña (Fig. 8f). Remarkable is that in west China (Xinjiang Province), the volcano-induced wetness is absent after La Niña events, although La Niñas do not cause dryness here. Thus, the major mutual interaction of volcanoes

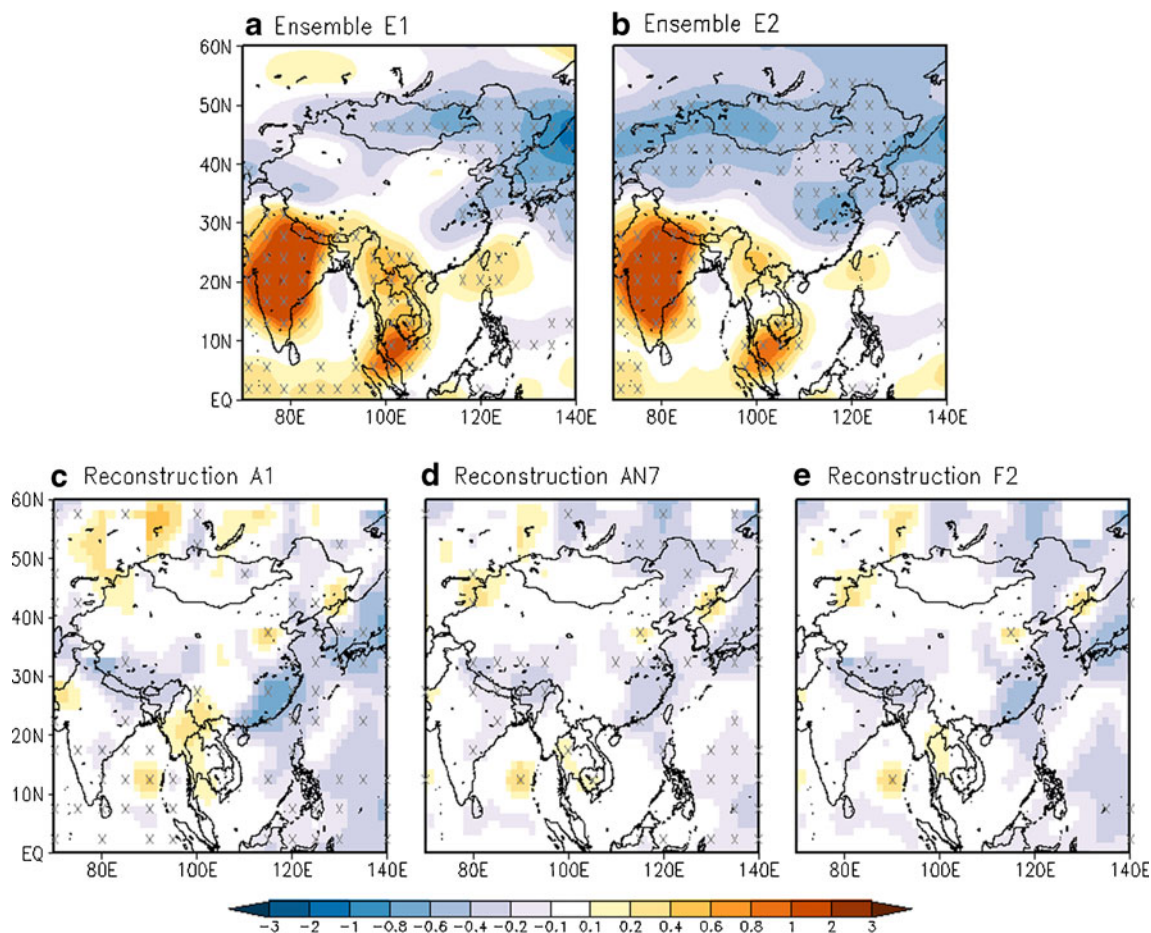


**Fig. 9** As Fig. 6 for volcanic eruptions with El Niño events. Reconstructions (c–e) are according to the list c A1 (Ammann et al. 2007); d AN7 (Ammann and Naveau 2003); and e F2 (Fischer et al. 2007, see Table 2)

and ENSO anomalies can be understood as a linear superposition, with a few deviations, mainly in west China, which can possibly be interpreted as nonlinearities. The SPI (JJA) anomalies obtained in the second ensemble E2 (not shown) show similar results. The average summer rainfall anomaly in China in the year after an eruption and a subsequent El Niño event in ensemble E1 is  $-64$  mm/month (E2,  $-68$  mm/month); for a subsequent La Niña event, the anomaly is even positive with  $29$  mm/month (E2,  $29$  mm/month).

Although there are suggestions that the GCMs may not completely capture the balance of important coupled ocean–atmosphere processes involved in the response of the Asian climate to radiative forcing (Anchukaitis et al. 2010), the reconstructions show similar tripole pattern in the simulations for all three lists (Fig. 10c–e): drier conditions in Mongolia, Northeast China, and South Asia and wetter conditions in central and Northeast China. Discrepancies between simulations and reconstructions occur in Northwest China and Mongolia. A noteworthy result is that compared to the volcanic effects with neutral ENSO events, the reconstruction reveals that the El Niño events after volcanic eruptions affect

mainly central and Northeast China (compare Fig. 7c–e with Fig. 10c–e) while the simulation indicates the El Niño impacts in East China (compare Fig. 7a, b with Fig. 10a, b).

### 5 Tambora eruption in 1815

The Tambora eruption in April 1815 was the most intense eruption in historic times classified by the Volcanic Explosivity Index=7 (on a scale from 0 to 8, see also Table 1). The Tambora eruption occurred during the Dalton minimum (1790–1830), an extreme cold period terminating the Little Ice Age and caused the year without summer in 1816. In the present simulations, the Tambora eruption is the second most intense with a drop in solar radiation of  $-6.9$  to  $-7.5$   $\text{W/m}^2$  detected in the eight ensemble members.

The eruption of the Tambora caused a long cold period in China. The temperature reduction (Fig. 11a) during the period 1780–1850 is clearly visible in the simulated annual mean temperature anomaly and in the reconstructions by Yang et al. (2002), Wang et al. (2007), and Mann et al. (2009). In this period, cold winters are reconstructed (Ge et

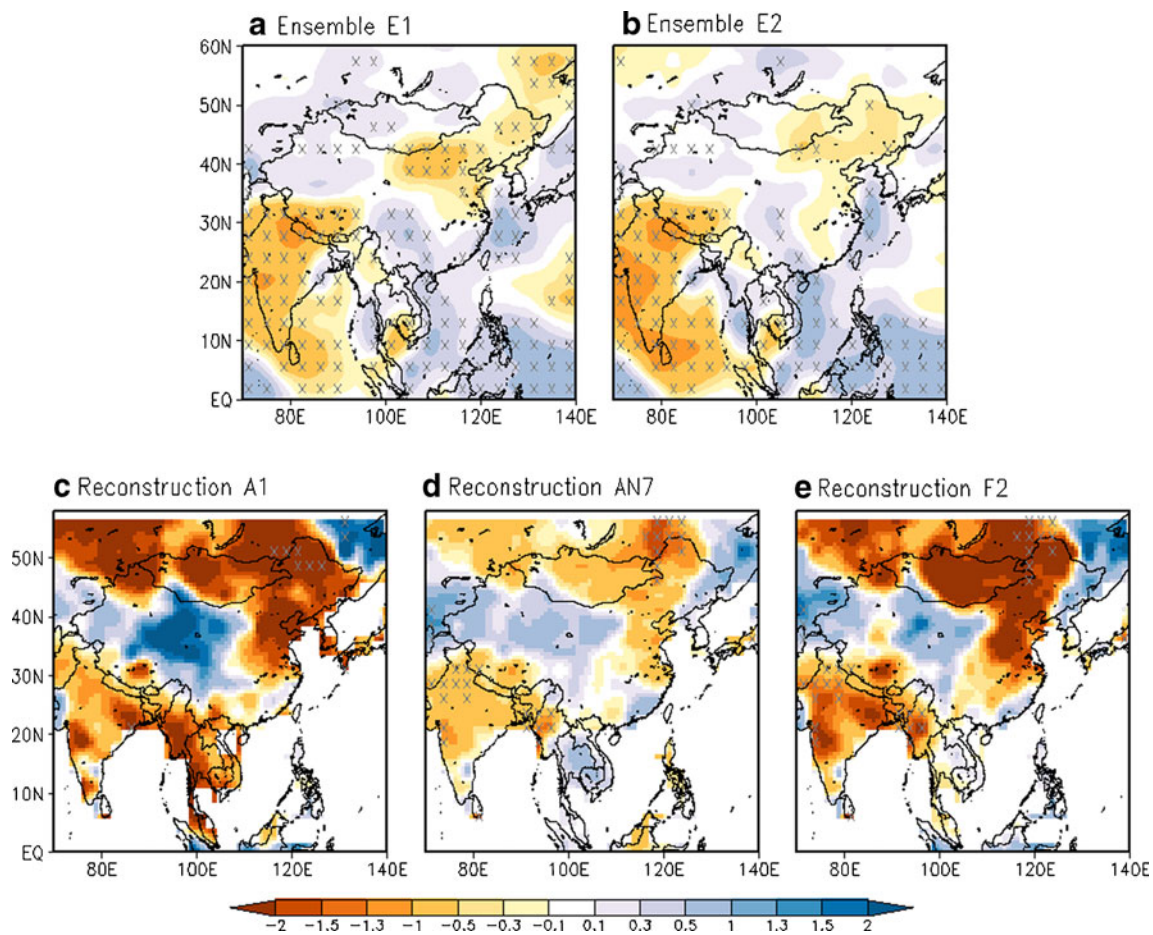


**Fig. 10** As Fig. 7 for volcanic eruptions with El Niño events. Reconstructions (c–e) are according to the list c A1 (Ammann et al. 2007); d AN7 (Ammann and Naveau 2003); and e F2 (Fischer et al. 2007, see Table 2)

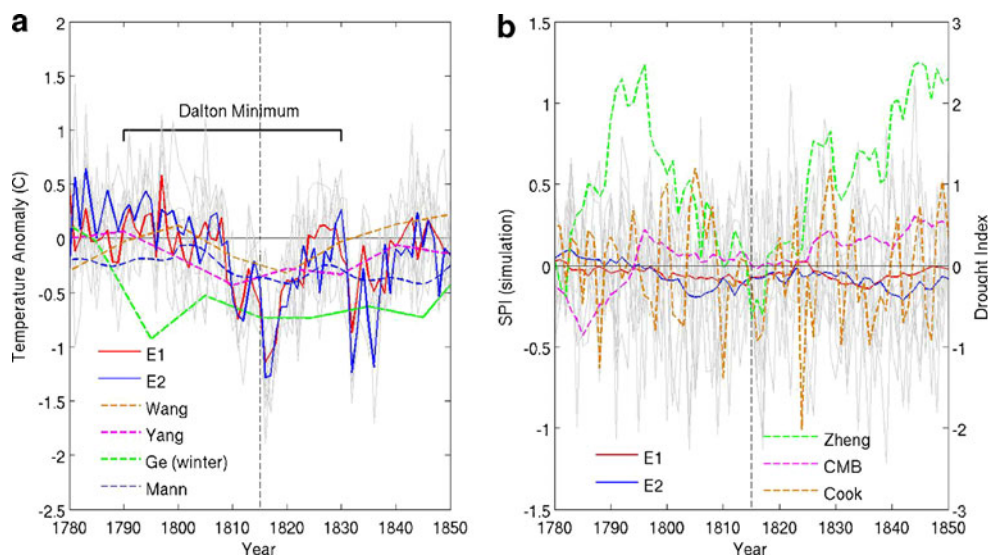


**Fig. 11 a** Temperature anomalies in China in simulations and reconstructions for 1780–1850. The Dalton Minimum (1790–1830) and the Tambaora eruption (1815) are marked. The simulated (*solid*) curves are ensemble means for E1 and E2; *thin gray lines* indicate all eight ensemble members, and the *dashed lines* refer to reconstructions by Yang et al.

(2002), Ge et al. (2003), Wang et al. (2007), and Mann et al. (2009). **b** Decadal mean Standardized Precipitation Index (SPI) for summers (*solid*, as in **a**, *left axis*) and reconstructed drought indices in Southeast China (*dashed*, *right axis*, Central Meteorological Bureau (CMB) 1981; Zheng et al. 2006; and Cook et al. 2010, annual means)

al. 2003). The cooling starts in 1809 (eruption of St. Helen) and reaches anomalies between  $-1.2$  and  $-1.3^{\circ}\text{C}$  in 1816 in the two ensembles. The simulated anomalies and the reconstruction by Mann et al. (2009) reveal recovery time scales of several years, which are distinctly longer than the mean calculated for 31 eruptions (Fig. 5b).

The summer (JJA) SPI in the simulations in Southeast China ( $105^{\circ}$ – $130^{\circ}$  E,  $25^{\circ}$ – $30^{\circ}$  N, the same region as in the reconstruction by Zheng et al. 2006) is below the mean for more than two decades, 1795–1825, in both simulations, which add up to a climatological relevant humidity deficit at the end of the Dalton minimum (Fig. 11b). The reconstruction of an annual drought index by the CMB (1981) averaged over Southeast China reveals high intra-annual variability and no relationship to the eruption in 1815. The decadal reconstructed summer drought index in Zheng et al. (2006) which is based on historical documents and the annual drought index in Cook et al. (2010) reveal depressions during the Dalton Minimum which are neither reflected in the CMB index nor in the simulation.

A SPI in the eight ensemble members reveals that there is a possible likelihood for decreased precipitation after 1815. Its variability can be explained by ENSO (see Figs. 7 and 10). Therefore, the eight PC1-SST time series in the period embedding the eruption (Fig. 12a) are compared to historic documents. Furthermore, extreme La Niña and El Niño events as well as a neutral case are considered.

In the reconstructed El Niño data (Quinn 1993), there were no El Niño events in 1815 and 1816, but probably strong El Niño events in 1814 and 1817. In the respective

time period, the reconstruction by McGregor et al. (2010) represents an El Niño in 1815/1816 which deviates from Quinn (1993). The data of Mann et al. (2009) do not contradict Quinn (1993). For a comparison, four simulations with different ENSO states are selected out of the eight members in the ensembles E1 and E2: (1) a neutral ENSO in 1813–1816 (simulation E1-3), (2) a strong El Niño in 1816 (E1-4) which follows the reconstructed ENSO by McGregor et al. (2010), (3) a strong La Niña in 1816 (E1-2), and (4) an optimal realization which follows the historically reconstructed El Niño events by Quinn (1993) closely during 1814–1817 (E2-3, Fig. 12a). Note that although we favor the widely accepted reconstruction by Quinn (1993, referred to as “Optimal”), we consider the data from McGregor et al. (2010) as well (E1-4, referred to as “El Niño”). Due to the absence of information about La Niña events, the reconstruction by Quinn (1993) does not exclude La Niña events in 1815 and 1816.

The simulations selected above reveal distinct patterns of temperature and precipitation anomalies in China during the decade 1810–1820 (Fig. 12b, c). A remarkable result is that the coldest simulated temperature anomalies for the optimal realization of the ENSO did not occur in 1816, but two years after the eruption, with a magnitude similar to the La Niña state. This persistence may explain long-lasting impacts like the 3 years famine in Yunnan Province.

Temperature and precipitation anomalies corresponding to the four ENSO states reveal different response patterns in East Asia in 1816 (Fig. 13, significance is given if the anomalies are larger than twice the standard deviation,

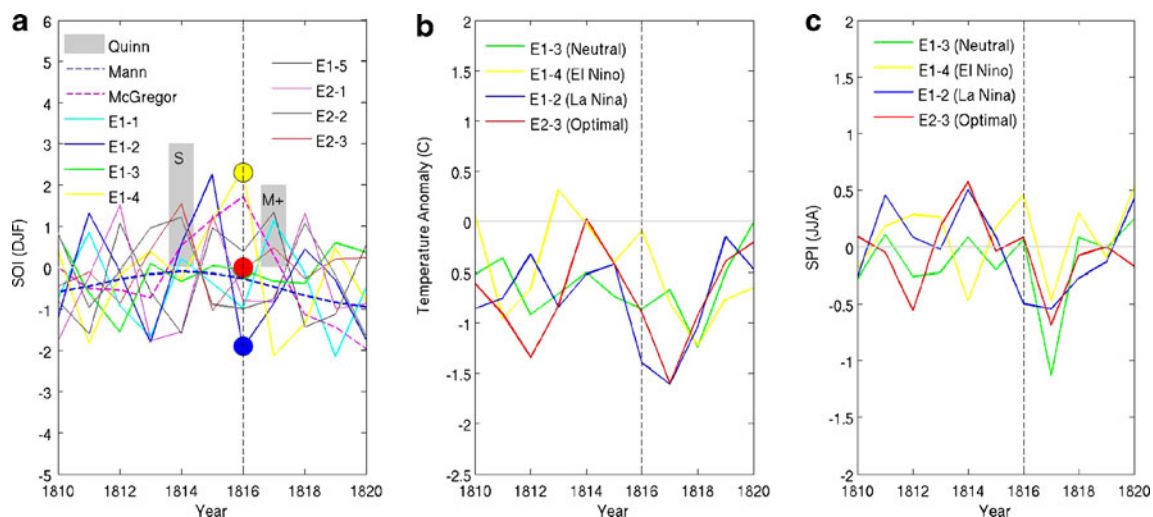


**Fig. 12** ENSO (PC1-SST) and climate in China during the cold decade of 1810 to 1820 embedding the year without summer (1816): **a** PC1-SST in eight members of the ensembles E1 and E2; gray shades with (*S*) and (*M+*) indicate “strong” and “moderate+” reconstructed El Niño events, respectively (see the definition by Quinn 1993); dashed lines are reconstructed ENSO by Mann et al. (2009) and McGregor et

al. (2010); dots are selected ENSO patterns: E1-3 (neutral, green, hidden by the red symbol), E1-4 (El Niño, yellow, following McGregor et al. 2010), E1-2 (La Niña, blue), E2-3 (optimal, red, following Quinn 1993); **b** annual temperature anomalies in China; and **c** summer SPI in Southeast China for selected ENSO patterns, curves as in **a**

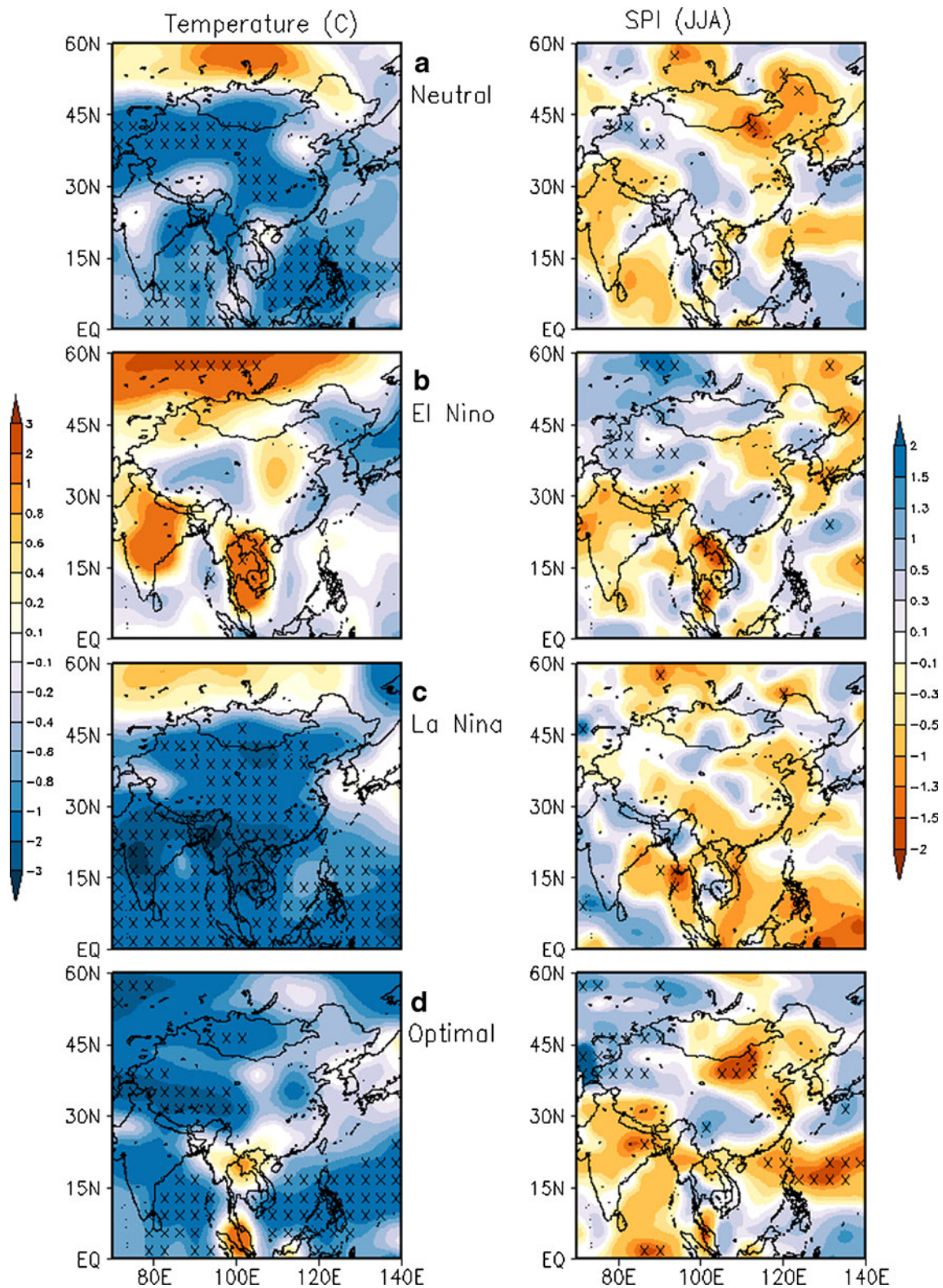


**Fig. 13** Temperature anomalies in 1816 (annual mean (in degree Celsius), *left column*) and SPI (JJA, *right column*) in four simulations with different ENSO patterns (see also Fig. 12): **a** neutral ( $|\text{PC1-SST}| < 1$ );

**b** El Niño (following McGregor et al. 2010); **c** La Niña; and **d** optimal realization (following Quinn 1993). Significant areas are marked (95 % level)

which is calculated independently for each ensemble member in the whole period 800–2005). (1) The neutral PC1-SST pattern shows a moderate cooling (compare with Fig. 6a–e) apart from Tibet, Northeast and Southeast China. The major impact is an extreme drought in East China (compare Fig. 7a–e); there is agreement with reconstructions in Northeast China (Mao et al. 2009). (2) The El Niño pattern (which is unlikely according to the reconstruction by Quinn 1993) balances the volcanic cooling and the dryness effects in large parts of China compared (Fig. 8a, d). (3) A La Niña state generates extreme coldness in East Asia and a moderate drought in the south and the northeast (i.e., the strong volcano dominates the La Niña impact, compare Fig. 8b, e). (4) The realization with the optimal ENSO pattern reveals a moderate cold anomaly in a large part of China (apart from the south) and an extreme drought in the northeast.

According to the comparison of the simulation with historical documents an El Niño event in the winter 1815/1816 can be excluded for two reasons (in agreement with Quinn 1993): first, observations report coldness in most parts of China while the El Niño simulation does not indicate a temperature anomaly; secondly, the documents describe droughts in the east as it is simulated by all ENSO states besides El Niño. However, a caveat remains for the simulation with the optimal ENSO (which is close to reconstructions) since the simulated wetness and the absence of a temperature anomaly in Southeast China contradict historical documents reporting a dry and cold period. A general conclusion is that temperature is dominated by the El Niño event, while precipitation remains dominated by the impact of the Tambora eruption.

## 6 Summary and discussion

Due to the high-population density, China is extremely vulnerable to the climate impacts of volcanic eruptions, in particular if at the same time East Asia is influenced by ENSO events which may amplify (but also mitigate) the anomalies caused by eruptions. The present analysis uses ensemble simulations with a comprehensive state of the art ESM and reconstructions to (1) determine the impact of eruptions on temperature and summer precipitation anomalies, (2) estimate the recovery time scales of temperature anomalies, and (3) analyze the correlations and the cooperative effects of volcanoes and ENSO events. A focus of this study was the Tambora eruption (1815) which had similar social impacts in China as the year without summer in Europe and North America. The ENSO states in different ensemble members are compared to historic information in 1814–1817 to select an optimal realization of the simulated climate. The main results are:

1. Volcanoes without ENSO events. A global cooling is found as well as a nonsignificant El Niño-like warming in the tropical Pacific Ocean. The following winter is warmer in parts of the Arctic Ocean, the tropical Pacific, the Bering Sea, the southern Pacific Ocean, Siberia, and in Central Asia. The recovery time scales of the cooling which describe the accumulated impact of the eruptions are determined locally by fitting an exponential function,  $\Delta T_0 \exp(-t/\tau)$ , with an amplitude  $\Delta T_0$  and a time scale  $\tau$ . The recovery time varies between 1 and 12 years globally with the shortest times found on the oceans. In China, the cooling decays mostly within the first 4 years, in the northeast, however, 10 years are detected. In East Asia, volcanoes cause a dramatic cooling in west China accompanied by drought in the eastern parts during the year after the eruption. The mean temperature is reduced by  $-0.54^\circ\text{C}$  in China and summer precipitation decreases by about  $-45$  mm/month. The reconstructions show similar cooling patterns with smaller magnitudes and confirm the drought in East China.
2. El Niño events without eruptions. After El Niño events warming is found in most parts of China apart from the northeast. The summer precipitation decreases in the north, while South China becomes wetter. La Niña events cause opposite effects for temperature and precipitation.
3. Volcanic eruption and ENSO events. The simulated occurrence of El Niño events is not significantly increased after volcanic eruptions. As this result appears to be in disagreement with reconstructions (Adams et al. 2003), it may be model specific. El Niño events after eruptions yield moderate temperature anomalies in China in simulations (consistent with reconstructions), in particular the volcano-induced cooling in the west is almost compensated by El Niño and the precipitation deficit in the southeast is inhibited. Both the simulated and reconstructed drought indices show tripole patterns which are altered by El Niño. La Niña events after eruptions, however, intensify the cooling (anomalies up to  $-3^\circ\text{C}$ ) and the drought in Southeast Asia. The cooperative impact of volcanic eruptions and ENSO cannot be considered as a linear superposition of two distinct signals in East Asia. Note that, although the pattern of the precipitation response to ENSO is captured in ECHAM5 simulations, the amplitude of the variations is slightly larger than observed (Hagemann et al. 2006). One of the model weaknesses is its regularity of 3–4 years (Blender et al. 2011), while observations indicate a variability of 2–7 years (Guilyardi et al. 2009). Furthermore, the present simulation reveals central Pacific ENSO anomalies (see Guilyardi et al. 2009).
4. Tambora eruption (1815). The climate response depends crucially on the ensemble member's state of ENSO. One

of the simulations yields an ENSO pattern which can be associated with the historical El Niño reconstruction (Quinn 1993; note that La Niña events are not documented). This simulation caused a moderate temperature anomaly of  $-1.2^{\circ}\text{C}$ , moderate wetness in South China, and extreme drought in the north and the northeast. Clearly, the results are constrained to a single optimal simulation; a large number of ensemble members in agreement with the optimal selection of ENSO would reduce the remaining internal noise and increase the credibility of the outcome.

Given the same definition of volcanic eruptions, the difference between the two ensembles E1 and E2 is small. The noticeable exception is the amplitude of winter temperature after eruptions. Aspects which are not considered in the current work are the locations and the intensities of the volcanic eruptions, which should be analyzed in future case studies or in simulations with larger numbers of ensemble members. As an outlook, we like to point out that the dynamics underlying the response to the extreme external inputs may be different in observations and simulations, not unlike the dynamic causes of extremes like drought and wetness which may also be different for observations and simulations (Bothe et al. 2011) with obvious consequences for the estimation of climate change.

**Acknowledgments** We acknowledge the valuable comments of the anonymous reviewer. We thank Johann Jungclaus, Martin Claußen, Xiuhua Zhu, and the Millennium consortium at the Max Planck Institute and at the University of Hamburg for providing the simulated data and stimulating discussions. We are grateful to Wang Shao-Wu (Beijing), Ge Quan-Sheng (Beijing), and Michael E. Mann (Pennsylvania State) for providing the reconstructed temperature and Zheng Jing-Yun, Anthony Garnaut, and Edward R. Cook (New York) for drought indices. DZ acknowledges the support for the visit to KlimaCampus by the Institute of Geographic Sciences and Natural Resources Research (Chinese Academy of Sciences) and KF acknowledges the support by the Max Planck Society.

## References

- Adams JB, Mann ME, Ammann CM (2003) Proxy evidence for an El Niño-like response to volcanic forcing. *Nature* 426:274–278
- Ammann CM, Naveau P (2003) Statistical analysis of tropical explosive volcanism occurrences over the last 6 centuries. *Geophys Res Lett* 30:1210. doi:10.1029/2002GL016388
- Ammann CM, Joos F, Schimel DS, Otto-Bliesner BL, Tomas RA (2007) Solar influence on climate during the past millennium: results from transient simulations with the NCAR Climate System Model. *Proc Natl Acad Sci USA* 104:3713–3718
- Anchukaitis KJ, Buckley BM, Cook ER, Cook BI, D'Arrigo RD, Ammann CM (2010) Influence of volcanic eruptions on the climate of the Asian monsoon region. *Geophys Res Lett* 37:L22703. doi:10.1029/2010GL044843
- Angell JK, Korshover J (1985) Surface temperature changes following the six major volcanic episodes between 1789 and 1980. *J Clim Appl Meteorol* 24:937–951
- Atwell WS (2001) Volcanism and short-term climatic change in East Asian and world history, c 1200–1699. *J World Hist* 12:29–98
- Bard E, Raisbeck G, Yiou F, Jouzel J (2000) Solar irradiance during the last 1200 years based on cosmogenic nuclides. *Tellus* 52B:985–992
- Blender R, Zhu X, Zhang D, Fraedrich K (2011) Yangtze runoff, precipitation, and the East Asian monsoon in a 2800 years climate control simulation. *Quatern Int* 244:194–201. doi:10.1016/j.quaint.2010.10.017
- Bordi I, Fraedrich K, Jiang J, Sutera A (2004) Spatio-temporal variability of dry and wet periods in eastern China. *Theor Appl Climatol* 79:81–91. doi:10.1007/s00704-004-0053-8
- Bothe O, Fraedrich K, Zhu X (2011) Large-scale circulations and Tibetan Plateau summer drought and wetness in a high-resolution climate model. *Int J Climatol* 31:832–846. doi:10.1002/joc.2124
- Brovkin V, Lorenz SJ, Jungclaus J, Raddatz T, Timmreck C, Reick CH, Segschneider J, Six K (2010) Sensitivity of a coupled climate-carbon cycle model to large volcanic eruptions during the last millennium. *Tellus* B 62:674–681. doi:10.1111/j.1600-0889.2010.00471.x
- Camp CD, Tung KK (2007) Surface warming by the solar cycle as revealed by the composite mean difference projection. *Geophys Res Lett* 34:L14703
- Central Meteorological Bureau (1981) Yearly charts of dryness/wetness in China for the last 500 years (in Chinese). Cartographic, Beijing
- Cole-Dai J, Ferris D, Lanciki A, Savarino J, Baroni M, Thieme MH (2009) Cold decade (AD 1810–1819) caused by Tambora (1815) and another (1809) stratospheric volcanic eruption. *Geophys Res Lett* 36:L22703
- Compo GP, Sardeshmukh PD (2010) Removing ENSO-Related variations from the climate record. *J Climate* 23:1957–1978
- Cook ER, Anchukaitis KJ, Buckley BM, D'Arrigo RD, Jacoby GC, Wright WE (2010) Asian monsoon failure and megadrought during the last millennium. *Science* 328:486–489. doi:10.1126/science.1185188
- Crowley TJ, Zielinski G, Vinther B, Udisti R, Kreutz K, Cole-Dai J, Castellano E (2008) Volcanism and the Little Ice Age. *PAGES News* 16:22–23
- D'Arrigo R, Wilson R, Tudhope A (2009) The impact of volcanic forcing on tropical temperatures during the past four centuries. *Nat Geosci* 2:51–56
- Dai J, Mosley-Thompson E, Thompson LG (1991) Ice core evidence for an explosive tropical volcanic eruption 6 years preceding Tambora. *J Geophys Res* 96:17361–17366
- Emile-Geay J, Seager R, Cane MA, Cook ER, Haug GH (2008) Volcanoes and ENSO over the past millennium. *J Climate* 21:3134–3148
- Fischer EM, Luterbacher J, Zorita E, Tett SFB, Casty C, Wanner H (2007) European climate response to tropical volcanic eruptions over the last half millennium. *Geophys Res Lett* 34:L05707. doi:10.1029/2006GL027992
- Foley JA, Costa MH, Delire C, Ramankutty N, Snyder P (2003) Green surprise? How terrestrial ecosystems could affect Earth's climate. *Front Ecol Environ* 1:38–44
- Fraedrich K, Blender R (2003) Scaling of atmosphere and ocean temperature correlations in observations and climate models. *Phys Rev Lett* 90:108501
- Fraedrich K, Blender R, Zhu X (2009) Continuum climate variability: long-term memory, extremes, and predictability. *Int J Mod Phys B* 23:5403–5416
- Friedlingstein P, Cox P, Betts R, Bopp L, von Bloh W, Brovkin V, Cadule P, Doney S, Eby M, Fung I, Bala G, John J, Jones C, Joos F, Kato T, Kawamiya M, Knorr W, Lindsay K, Matthews HD, Raddatz T, Rayner P, Reick C, Roeckner E, Schnitzler KG,

- Schnur R, Strassmann K, Weaver AJ, Yoshikawa C, Zeng N (2006) Climate-carbon cycle feedback analysis: results from the C<sup>4</sup>MIP model intercomparison. *J Climate* 19:3337–3353
- Froelicher TL, Joos F, Raible CC (2011) Sensitivity of atmospheric CO<sub>2</sub> and climate to explosive volcanic eruptions. *Biogeosci* 8:2317–2339
- Ge QS, Zheng JY, Fang XQ, Man ZM, Zhang XQ, Zhang PY, Wang WC (2003) Winter half-year temperature reconstruction for the middle and lower reaches of the Yellow River and Yangtze River, China, during the past 2,000 years. *Holocene* 13:933–940
- Gergis J, Fowler A (2006) How unusual was late 20th century El Niño–Southern Oscillation (ENSO)? Assessing evidence from tree-ring, coral, ice-core and documentary palaeoarchives, AD 1525–2002. *Adv Geosci* 6:173–179
- Global Volcanism Program (2011) Smithsonian National Museum of Natural History/Washington: Available at [http://www.volcano.si.edu/world/find\\_eruptions.cfm](http://www.volcano.si.edu/world/find_eruptions.cfm). Accessed 1 November 2011
- Goosse H, Renssen H, Timmermann A, Bradley RS, Mann ME (2006) Using paleoclimate proxy-data to select optimal realizations in an ensemble of simulations of the climate of the past millennium. *Clim Dynam* 27:165–184. doi:10.1007/s00382-006-0128-6
- Guilyardi E, Wittenberg A, Fedorov A, Collins M, Wang C, Capotondi A, van Oldenborgh GJ, Stockdale T (2009) Understanding El Niño in ocean–atmosphere general circulation models: progress and challenges. *Bull Amer Meteorol Soc* 90:325–340
- Hagemann S, Arpe K, Roeckner E (2006) Evaluation of the hydrological cycle in the ECHAM5 Model. *J Climate* 19:3810–3827
- Hoerling MP, Kumar A, Xu T (2001) Robustness of the nonlinear climate response to ENSO's extreme phases. *J Climate* 14:1277–1293
- Jiang T, Zhang Q, Blender R, Fraedrich K (2005) Yangtze Delta floods and droughts of the last millennium: abrupt changes and long term memory. *Theor Appl Climatol* 82:131–141
- JungCLAUS JH, Lorenz SJ, Timmreck C, Reick CH, Brovkin V, Giorgetta MA, Raddatz TJ, Roeckner E, Segsneider J, Six K, Schnur R, Widmann H, Crowley TJ, Krivova N, Vieira LE, Solanki SK, Klocke D, Botzet M, Esch M, Gayler V, Haak H, Pongratz J, Claussen M, Stevens B, Marotzke J (2010) Climate and carbon-cycle variability over the last millennium. *Clim Past* 6:1009–1044
- Kirchner I, Graf HF (1995) Volcanos and El Niño: signal separation in Northern Hemisphere winter. *Clim Dynam* 11:341–358
- Krivova NA, Balmaceda L, Solanki SK (2007) Reconstruction of solar total irradiance since 1700 from the surface magnetic flux. *Astron Astrophys* 467:335–346
- Lean JL, Rind DH (2008) How natural and anthropogenic influences alter global and regional surface temperatures: 1889 to 2006. *Geophys Res Lett* 35:L18701
- Mann ME, Cane MA, Zebiak SE, Clement A (2005) Volcanic and solar forcing of the Tropical Pacific over the past 1000 years. *J Climate* 18:447–456
- Mann ME, Zhang Z, Rutherford S, Bradley R, Hughes MK, Shindell D, Ammann C, Faluvegi G, Ni F (2009) Global signatures and dynamical origins of the Little Ice Age and Medieval climate anomaly. *Science* 326:1256–1260. doi:10.1126/science.1177303
- Mao X, Cheng S, Hong Y, Zhu Y, Wang F (2009) The influence of volcanism on paleoclimate in the northeast of China: insights from Jinchuan peat, Jilin Province, China. *Chin J Geochem* 28:212–219. doi:10.1007/s11631-009-0212-9
- Marsland S, Haak H, JungCLAUS JH, Latif M, Röske F (2003) The Max-Planck-Institute global ocean/sea ice model with orthogonal curvilinear coordinates. *Ocean Model* 5:91–127
- Mass CF, Portman DA (1989) Major volcanic eruptions and climate: a critical evaluation. *J Climate* 2:566–593
- McGregor S, Timmermann A, Timm O (2010) A unified proxy for ENSO and PDO variability since 1650. *Clim Past* 6:1–17
- McKee TB, Doesken NJ, Kleist J (1993) The relationship of drought frequency and duration to time scales. In: 8th Conf on applied climatology, Amer Meteor Soc Anaheim, Canada, 179–184
- Newhall CG, Self S (1982) The volcanic explosivity index (VEI): an estimate of explosive magnitude for historical volcanism. *J Geophys Res* 87:1231–1238
- Oppenheimer C (2003) Climatic, environmental and human consequences of the largest known historic eruption: Tambora volcano (Indonesia) 1815. *Prog Phys Geog* 27:230–259
- Peng Y, Shen C, Wang W, Xu Y (2010) Response of summer precipitation over Eastern China to large volcanic eruptions. *J Climate* 23:818–824. doi:10.1175/2009JCLI2950.1
- Penland C, Matrosova L (2006) Studies of El Niño and interdecadal variability in tropical sea surface temperatures using a nonnormal filter. *J Climate* 19:5796–5815
- Pongratz J, Reick C, Raddatz T, Claussen M (2008) A reconstruction of global agricultural areas and land cover for the last millennium. *Global Biogeochem Cy* 22:GB3018. doi:10.1029/2007GB003153
- Quinn WH (1993) The large-scale ENSO event the El Niño and other important regional features. *Bull Inst fr études andines* 22:13–34
- Raddatz TJ, Reick CJ, Knorr W, Kattge J, Roeckner E, Schnur R, Schnitzler KG, Wetzel P, JungCLAUS JH (2007) Will the tropical land biosphere dominate the climate-carbon cycle feedback during the 21st century. *Clim Dynam* 29:565–574
- Rampino MR, Self S (1982) Historic eruptions of Tambora (1815), Krakatau (1883), and Agung (1963), their stratospheric aerosols, and climatic impact. *Quatern Res* 18:127–143
- Robock A (2000) Volcanic eruptions and climate. *Rev Geophys* 38:191–219
- Robock A, Liu Y (1994) The volcanic signal in Goddard Institute for space studies three-dimensional model simulations. *J Climate* 7:44–55
- Robock A, Mao J (1995) The volcanic signal in surface temperature observations. *J Climate* 8:1086–1103
- Robock A, Oman L, Stenchikov GL (2008) Regional climate responses to geoengineering with tropical and Arctic SO<sub>2</sub> injections. *J Geophys Res* 113:D16101. doi:10.1029/2008JD010050
- Roeckner E, Bäuml G, Bonaventura L, Brokopf R, Esch M, Giorgetta M, Hagemann S, Kirchner I, Kornbluh L, Manzini E, Rhodin A, Schlese U, Schulzweida U, Tompkins A (2003) The atmospheric general circulation model ECHAM5, Part I: model description. Max Planck Institute for Meteorology. Rep 349:1–127
- Santer BD, Wigley TML, Doutriaux C, Boyle JS, Hansen JE, Jones PD, Meehl GA, Roeckner E, Sengupta S, Taylor KE (2001) Accounting for the effects of volcanoes and ENSO in comparisons of modeled and observed temperature trends. *J Geophys Res* 106:28033–28059
- Schneider DP, Ammann CM, Otto-Bliesner BL, Kaufman DS (2009) Climate response to large, high-latitude and low-latitude volcanic eruptions in the Community Climate System Model. *J Geophys Res* 114:D15101. doi:10.1029/2008JD011222
- Shindell DT, Schmidt GA, Miller RL, Mann ME (2003) Volcanic and solar forcing of climate change during the preindustrial era. *J Climate* 16:4094–4107
- Shindell DT, Schmidt GA, Mann ME, Faluvegi G (2004) Dynamic winter climate response to large tropical volcanic eruptions since 1600. *J Geophys Res* 109:D05104. doi:10.1029/2003JD004151
- Sienz F, Bordi I, Fraedrich K, Schneidereit A (2007) Extreme dry and wet events in Iceland: observations, simulations and scenarios. *Meteorol Zeitschr* 16:9–16
- Sims AP, Niyogi DS, Raman S (2002) Adopting drought indices for estimating soil moisture: a North Carolina case study. *Geophys Res Lett* 29(8):1183. doi:10.1029/2001GL013343
- Soon W, Yaskell SH (2003) Year without a summer. *Mercury* 32:13–22
- Stenchikov G, Hamilton K, Stouffer RJ, Robock A, Ramaswamy V, Santer B, Graf HF (2006) Arctic Oscillation response to volcanic eruptions in the IPCC AR4 climate models. *J Geophys Res* 111:D07107. doi:10.1029/2005JD006286
- Stenchikov G, Delworth TL, Ramaswamy V, Stouffer RJ, Wittenberg A, Fanrong F (2009) Volcanic signals in oceans. *J Geophys Res* 114:D16104. doi:10.1029/2008JD011673

- Stothers RB (1984) The great Tambora eruption in 1815 and its aftermath. *Science* 224:1191–1198
- Thompson RD (1995) Volcanic eruptions and global temperatures. *Ambio* 24:320–321
- Timmreck C, Lorenz SJ, Crowley TJ, Kinne S, Raddatz TJ, Thomas MA, Jungclaus JH (2009) Limited temperature response to the very large AD 1258 volcanic eruption. *Geophys Res Lett* 36: L21708. doi:10.1029/2009GL040083
- Timmreck C, Graf HF, Lorenz SJ, Niemeier U, Zanchettin D, Matei D, Jungclaus JH, Crowley TJ (2010) Aerosol size confines climate response to volcanic supereruptions. *Geophys Res Lett* 37: L24705. doi:10.1029/2010GL045464
- Tung KK, Zhou J, Camp C (2008) Constraining model transient climate response using independent observations of solar cycle forcing and response. *Geophys Res Lett* 35:L17707
- Wang SW, Wen XY, Luo Y, Dong WJ, Zhao ZC, Yang B (2007) Reconstruction of temperature series of China for the last 1000 years. *Chin Sci Bull* 52:3272–3280
- Wetzel P, Maier-Reimer E, Botzet M, Jungclaus JH, Keenlyside N, Latif M (2006) Effects of ocean biology on the penetrative radiation in a coupled climate model. *J Climate* 19:3973–3987
- Yang B, Bräuning A, Johnson KR, Shi YF (2002) General characteristics of temperature variation in China during the last two millennia. *Geophys Res Lett* 29:1324–1327. doi:10.1029/2001GL014485
- Yang YD, Man ZM, Zheng JY (2005) A serious famine in Yunnan (1815–1817) and the eruption of Tambora Volcano (in Chinese). *Fudan J (Soc Sci)* 1:79–85
- Yoshimori M, Stocker TF, Raible CC, Renold M (2005) Externally forced and internal variability in ensemble climate simulations of the Maunder Minimum. *J Climate* 18:4253–4270
- Zhai J, Su B, Krysanova V, Vetter T, Gao C, Jiang T (2010) Spatial variation and trends in PDSI and SPI indices and their relation to streamflow in 10 large regions of China. *J Climate* 23:649–663
- Zhang D, Blender R, Zhu X, Fraedrich K (2010) Temperature variability in China in an ensemble simulation for the last 1200 years. *Theor Appl Climatol* 103:387–399. doi:10.1007/s00704-010-0305-8
- Zhang D, Blender R, Fraedrich K (2011) Volcanic and ENSO effects in China in simulations and reconstructions: Tambora eruption, 1815. *Clim Past Discuss* 7:2061–2088
- Zheng JY, Wang WC, Ge QS, Man ZM, Zhang PY (2006) Precipitation variability and extreme events in Eastern China during the past 1500 years. *Terr Atmos Ocean Sci* 17:579–592
- Zhu X, Bothe O, Fraedrich K (2010) Summer atmospheric bridging between Europe and East Asia: influences on drought and wetness on the Tibetan Plateau. *Quatern Int.* doi:10.1016/j.quaint.2010.06.015